Journal of Applied Polymer Science

REVIEW

CO_2-Blown Nanocellular Foams

Stéphane Costeux
The Dow Chemical Company, Dow Building Solutions, 1605 Joseph Dr., 200 Larkin Center, Midland, Michigan 48674
Correspondence to: S. Costeux (E-mail: sccosteux@dow.com)

ABSTRACT: Polymeric nanocellular foams are broadly defined as having cell size below one micron. However, it is only when cell size reaches 100 nm or less that unique thermal conductivity, dielectric constant, optical, or mechanical properties are expected due to gas confinement in the cells or polymer confinement in the cell walls. Producing such materials with low density by physical foaming with CO_2 requires the controlled nucleation and growth of $10^{15}-10^{16}$ cells/cm^3. This is a formidable challenge that necessitates new foaming strategies. This review provides a description of processes, conditions, and polymer systems that have been employed over the past 15 years to achieve increasingly higher cell densities and expansion ratio, culminating with the recent development of low density nanofoams and of nanostructured polymers in which nucleation can be precisely controlled. Remaining barriers to scale-up are summarized. © 2014 Wiley Periodicals, Inc. J. Appl. Polym. Sci. **2014**, *131*, 41293.

KEYWORDS: foams; nanostructured polymers; porous materials; thermal properties

Received 29 May 2014; accepted 24 July 2014
DOI: 10.1002/app.41293

INTRODUCTION

In recent years, nanostructured materials have been the new frontier for materials and polymer science.

Nanoscale objects can act as nanofillers and contribute to enhancement of mechanical properties when adequately dispersed.[1] Their presence affects the stability of interfaces, resulting in remarkable properties such as superhydrophobicity[2] that would not be achieved by the use of micron-scale objects.

This distinction extends to porous or cellular materials. Unusual properties exist due to nanometer-scale confinement of the solid, or of the medium (air, gas, or liquid) contained within the pores or cells, or owing to surface effects at nanostructured interfaces between polymer and medium. For instance, the presence of nanoscale voids and nanoscale distribution of the solid material in silica aerogels has long been known to be responsible for their unique properties, in particular their low thermal conductivity (TC).[3]

Quite naturally, various techniques have been considered to achieve polymeric structures with nanopores. Sol–gel techniques have been applied toward the production of organic aerogel with TC or mechanical properties that approach or exceed those of inorganic aerogels.[3] Other methods to produce nanoporous structures involve the use of a porogen component or block copolymers with sacrificial blocks,[4–6] colloidal assembly, microemulsion templating,[7] or crosslinked polymer networks. These techniques require solvents that have to be subsequently removed, or the use of freeze drying.[8] Yet an important challenge is to produce such structures by "sustainable" processes which minimize the use of solvents and sacrificial blocks, and minimize the energy or time needed to produce the nanoporous structure (solvent exchange and supercritical drying of aerogels). Effort to use CO_2 as a green solvent have had limited success.[9,10]

Recently, focus has been to build up on the advances in the development of microcellular foams that occurred in the 1980s,[11] and became commercial in the 2000s. CO_2-blown microcellular foams, defined as having average cell size between 1 and 10 μm, were initially produced by a batch foaming process. They showed property benefits over regular foams. For instance, microcellular foaming allowed for weight reduction (10–30%) with minimal decrease in mechanical strength.[12] Because of the cells' ability to interfere with crack propagation, impact properties and toughness were improved compared to unfoamed polymer. The conversion of this technology to a continuous process by injection molding and its application to the production of light weight parts with a variety of materials have been one of the most significant advances in foams in the past 30 years.

It is expected that physical foaming with CO_2 can produce nanocellular foams with cells as small as 100 nm that will rival properties of solvent-based nanoporous materials, in particular low density nanofoams for light-weighting and thermal insulation. To successfully produce nanocellular CO_2-blown foams, it

Stéphane Costeux is a Research Scientist/Leader at The Dow Chemical Company in the Building & Construction business unit. He graduated as R&D engineer from ESPCI-ParisTech (France), obtained a Ph.D. in Physics of Liquids from University Paris VI in 1999 and was a postdoctoral fellow at McGill University for two years. He joined Dow Plastics R&D in 2002. His main research focuses on polymer design for improved processability and materials development for new foam applications.

is necessary to generate, grow and stabilize $10^{15}-10^{16}$ cells/cm^3 of the unfoamed material, compared with 10^9-10^{12}/cm^3 for microcellular foams. The following sections outline strategies, processes and polymer systems used to achieve this objective. Polymer acronyms are defined in the "Abbreviations" section.

STRATEGIES TO GENERATE NANOSCALE CELLS WITH CO_2

Conventional CO_2 physical foaming is the pathway by which an equilibrated polymer/CO_2 mixture at high enough pressure to maintain CO_2 in solution transitions to a stable two-phase (solid/gas) system at ambient temperature and pressure. The pathway differs depending on how the pressure is decreased or on the evolution of temperature, but the mechanism generally occurs in three stages.

The initial stage is a phase separation event, which can be triggered by a sudden pressure decrease or by an increase in temperature causing supersaturation. Two major mechanisms are known to occur in new phase formation, such as the formation of a bubble in a polymeric material.[13] One is spinodal decomposition in which a wavelike concentration fluctuation with periodic wavelength increases over time, producing a cocontinuous structure. This mode can occur when a liquid-liquid phase separation is induced by a temperature change before the pressure is dropped. Since CO_2 solubility in most polymers is higher at lower temperatures, a temperature increase is generally used to trigger spinodal decomposition. The other is nucleation, which occurs when the temperature and pressure in the supersaturated state fall in the metastable region between the binodal and the spinodal. Due to the position of the spinodal in polymer-CO_2 systems[14] a drop in pressure almost always leads to nucleation. The second stage is the growth of newly formed stable nuclei into bubbles or cells. Cell nucleation and growth can occur simultaneously or successively. The third stage is the stabilization, where conditions are controlled to freeze the foam structure.

Controlling or Avoiding Nucleation

Guidance from the Classical Nucleation Theory. Nucleation is a kinetic phenomenon. The rate of nucleation in foams is often described using the Classical Nucleation Theory (CNT). The theory, initially developed for liquid/vapor systems, expresses the energy of the system as the sum of a bubble surface contribution, depending on the interfacial tension γ_{bp} between the bubble and the polymer-rich phase, and a volume contribution proportional to the pressure difference ΔP between the bubble and the bulk. Stability analysis yields a Gibbs free energy barrier

$$\Delta G^*_{hom} = \frac{16\pi}{3\Delta P^2}\gamma^3_{bp} \quad (1)$$

which needs to be overcome for nuclei to grow into stable bubbles of size R exceeding the critical nucleus radius $R^* = 2\gamma_{bp}/\Delta P$. The homogeneous nucleation rate (bubble formation rate) is then[15]

$$J = f_0 C_0 exp\left[-\frac{\Delta G^*_{hom}}{kT}\right] \quad (2)$$

where C_0 is the concentration of CO_2 and f_0 is the rate of production of nuclei.[16] This simplified theory predicts that higher CO_2 concentrations are beneficial, as they decrease the interfacial tension[14] γ_{bp} and increase J. Higher pressure difference are also beneficial to reduce ΔG^*_{hom}. The rate J is a function of time, which will vanish once nucleation stops. Because of nuclei collapse and coalescence of growing bubbles, the total number of nuclei produced, defined as $N = \int J(t)dt$, will be larger than the number of effective nuclei, N_0, which will survive through the foaming process to form a cell in the final foam.

Qualitative trends for the effect of pressure, temperature, and CO_2 concentration on the nucleation density of binary polymer/CO_2 predicted by the CNT have generally been observed experimentally for microcellular foams.[16,17] These trends are expected to hold to some extend at the nanoscale, and mathematical foaming models using a form of the CNT in which f_0 is used as an adjustable parameter have shown promising results in predicting foaming at the nanoscale.[18] However, the CNT performs poorly in quantitatively predicting the absolute nuclei production rate, the absolute free energy barrier[19,20] or the maximum cell density[21,22] due in part to failure to capture the polymer/CO_2 interactions at the interface of nanoscale bubbles. Additional limitations have been reviewed by Lubetkin[23] and Tomasko et al.[24]

Heterogeneous Nucleation. Addition of nucleating particles is commonly practiced in conventional or microcellular foaming to enhance the nucleation density by providing heterogeneous surfaces on which the nucleation energy barrier is lowered.[25] Smaller particle size promotes higher nucleation density by providing more nucleation sites at the same particle concentration. Interestingly, Ramesh and Lee[26] showed that nanoparticles are rather ineffective in the nucleation of conventional PP foams. Spitael et al.[27] made a similar observation when adding PS-*b*-PEP block copolymer micelles in an attempt to reduce the cell size of microcellular PS foams. Yet, there is evidence that even at the nanoscale, the principle of heterogeneous nucleation may apply,[28–30] provided that the right of type of nanoscale

nucleating agent and the optimal foaming conditions be chosen for each polymer to maximize nucleation.[31]

Effect of Pressure Drop Rate. The efficiency of cell nucleation is affected by nuclei coalescence. Zhu et al.[32] showed that pressure difference between small and larger nascent cells causes a ripening of the nuclei population by gas diffusion. This suggests that increasing the rate of nucleation, e.g., by increasing the pressure drop rate, may allow for survival of a larger number of stable nuclei before diffusion effects come into play due to narrower nuclei size distribution or additional internal cooling. The benefit of higher depressurization has been shown at the microcellular scale[33] and should still be significant at the nanoscale.

Bypassing Nucleation. The difficulty in controlling the generation of nuclei in a homogeneous polymer system has led researchers to seek methods to generate bubbles from templated multiphase polymer systems. Nanoscale templates can readily be produced by block copolymer self-assembly. The approach was pioneered by Yokoyama et al.,[34,35] who used diblock copolymers with a CO_2-philic fluorinated block to produce thin films with organized micelles structure. The high CO_2 solubility in the fluorinated micelles favored initiation of one bubble per micelle, thus providing an effective control of the cell density. The concept was also adapted to blends of polymers with block copolymers[36,37] or immiscible blends.[38,39]

Maximizing Foam Expansion. At the end of the nucleation, the nascent foam consists of a number of stable nuclei dispersed into the polymer/CO_2 mixture. To have a chance to produce nanocellular foams with reduced density after expansion of these nuclei, a successful nucleation stage should yield stable nuclei in excess of $N_0=10^{15}/\text{cm}^3$ (per cm^3 of unfoamed polymer). N_0 will be called the cell nucleation density, and refers to the number of effective nuclei that will result in an actual cell in the final foam (nuclei that disappear by coalescence or ripening before the end are ignored). It is a better measure of the cell density than N_c (number of cells per cm^3 of the final foam) because it is corrected by the expansion ratio r ($N_0=r\ N_c$).[40] If cells have an average diameter ϕ_{nm} (in nanometers), the expansion ratio and the foam porosity (void volume fraction), p, are given by

$$r=1+\frac{\pi\phi_{\text{nm}}^3 N_0}{6\times10^{21}} \quad \text{and} \quad p=\frac{r-1}{r} \tag{3}$$

The nascent foam can be modeled as a regular array of cubic cells. Prior to cell growth, cells in this model foam are nuclei with critical size $2R^*$, typically of the order of a few nanometers. The average distance between these nuclei is of the order of 100 nm, and the volume fraction they occupied (porosity p during nucleation) is less than 0.1%. As the model foam expands, each nucleus becomes a growing bubble. Figure 1 shows the evolution of the porosity and the distance between the surfaces of adjacent cells (the average wall thickness) as all cells expand simultaneously. It should be noted that N_c decreases during cell growth, whereas by design N_0 remains constant.

According to Figure 1, for $N_0=10^{15}/\text{cm}^3$ cells need to expand to a size of 200 nm to achieve 80% porosity, corresponding to an expansion ratio of 5. This requires stretching the cell walls between the cells down to a thickness of about 15 nm. For $N_0=10^{16}/\text{cm}^3$, 80% porosity is reached for 100 nm cells with 5 nm cell walls. These numbers emphasize the magnitude of the challenge in producing polymeric nanofoams. Polymer chains have to deform and become confined at dimensions similar to molecular size.

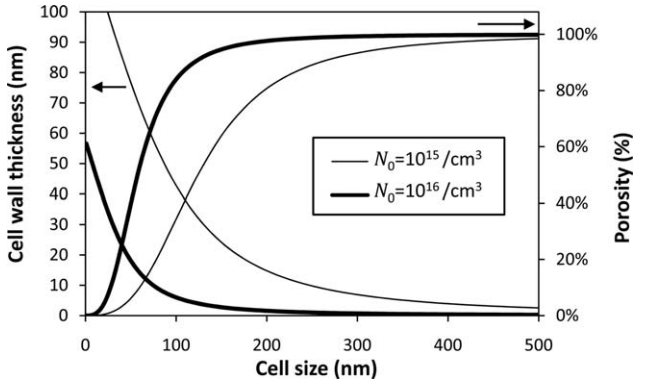

Figure 1. Relation between average cell size, porosity, and average cell wall thickness for a model foam with cubic cells and a fixed cell nucleation density.

Therefore, preventing cell coalescence during expansion is paramount. Cell ripening by diffusion needs to be prevented by reducing the expansion time (fast depressurization), by controlling the temperature to maintain very high viscosities,[41] or by manipulating the relative properties of the matrix and domains in multi-phase polymer systems, for instance by lowering the temperature below the glass transition temperature (T_g) of the matrix.[34] Lack of integrity of the cell walls can in some cases yield open cell foams, which is desirable in certain applications such as membranes.

In all cases, a stabilizing mechanism is needed to freeze the foam structure. Even if the temperature is not intentionally varied right before or during foaming, the Joule-Thomson effect resulting from the rapid expansion of CO_2 in the cells induces a rapid decrease of the temperature in the foam.[29] Another stabilizing effect relates to a decrease of the plasticization of the polymer by CO_2 as the gas diffuses into the growing cells. If the initial foaming temperature is chosen below the T_g of the pure polymer but above the T_g of the polymer plasticized by CO_2, the polymer/CO_2 mixture will eventually become glassy as the CO_2 concentration decreases during foaming.[42] The same strategy can be used with the crystallization temperature of semicrystalline polymers.

NANOFOAM PRODUCTION PROCESSES

The process to make nanofoam is inspired from the batch foaming process initially used to make microcellular foams[11] in the 1980s and 90s. In its most general form, the equipment consists of an autoclave that can be maintained at a set temperature, connected to a carbon dioxide source with pressure control (typically a syringe pump), and a valve to release the gas from the vessel. The autoclave containing the sample is conditioned at the "soak temperature" (or sorption temperature),

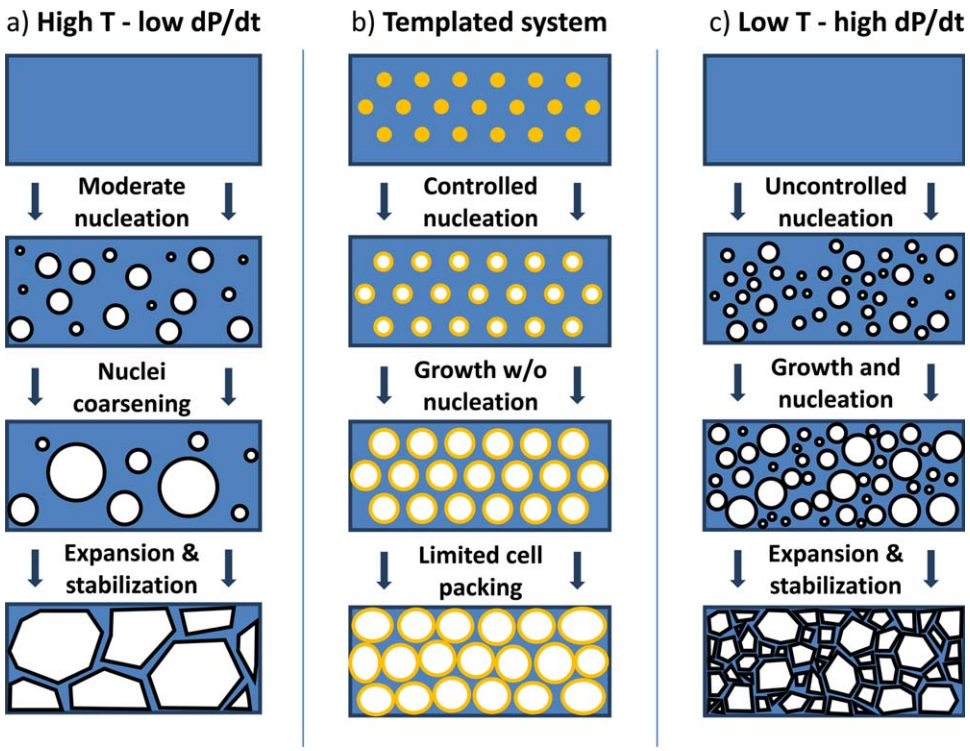

Figure 2. Strategies for microcellular and nanocellular foams; (a) homogeneous systems foamed under conditions of insufficient nucleation density or favoring nuclei ripening become microcellular foams. (b) Templated system under similar conditions remain nanocellular, but with low expansion (<2X); (c) Homogeneous system foamed under conditions favoring high nucleation and growth simultaneously can yield low density nanofoams. [Color figure can be viewed in the online issue, which is available at wileyonlinelibrary.com.]

CO_2 is fed into the autoclave and the pump is activated to progressively increase the CO_2 pressure in the autoclave. The sorption conditions are maintained until the CO_2 concentration in the sample reaches the solubility limit at the soaking conditions. The minimum soaking time has to be determined either empirically or by calculation[43] using the CO_2 diffusion coefficient in the particular polymer at the soaking conditions and the sample thickness. It varies from less than an hour for thin samples (100 μm or less) to several days for thick samples at low temperature.

Upon equilibration, the release valve is opened to remove CO_2. The pressure decrease triggers nucleation, but not necessarily foam expansion. In the case of microcellular foams, soaking could be done at temperature higher than the T_g or right above the T_m of the polymer, and depressurization would induce both nucleation and foam expansion. However, these conditions generally do not produce high enough cell nucleation densities to generate nanocellular foams [see Figure 2(a)]. Therefore, CO_2-blown nanofoams are more likely produced by soaking at temperatures lower than the T_g of the polymer when it is amorphous, and slightly below T_m when it is semicrystalline.

CO_2 solubility in amorphous polymers generally increases as the temperature is decreased, so that at the soaking temperature, the CO_2-laden polymer can be either glassy or rubbery. In the former case, upon depressurization, nucleation will take place but little expansion will be observed. The specimen retrieved from the autoclave may remain transparent. Foam expansion then requires a second step, where the temperature of the sample is increased (e.g., by immersion in a heated bath) to allow for expansion of nuclei into cells. Procedures involving this second thermal conditioning step will be called "two-step process" and denoted 2S in the following. The process is depicted in Figure 3(b).

If the polymer specimen becomes rubbery upon saturation with CO_2, the internal pressure in the nuclei formed during pressure release will deform the polymer matrix and allow foam expansion to occur. The diffusion of CO_2 out of the polymer matrix will eventually return the matrix to a glassy solid, at which point foam expansion will stop.[44] This procedure is called "one-step process" denoted 1S [Figure 3(a)].

Some variations of these two processes exist. For instance the 2S process can involve expansion in both the depressurization step and the thermal conditioning steps if soaking is done when the CO_2-laden polymer is in the rubbery regime.[45] Conversely, soaking can be done in the rubbery regime, but the temperature is decreased to turn the mixture glassy before pressure drop[34] with optionally a second thermal conditioning step to enhance expansion[29] [see Figure 3(c)].

At this time, few attempts have been made to produce nanocellular foams by continuous processes. Unlike microcellular foams, which can readily been produced by a high temperature, one-step foaming process suitable for extrusion or injection molding, stable nanofoam structures are more likely to be produced in a low temperature process. A successful attempt to

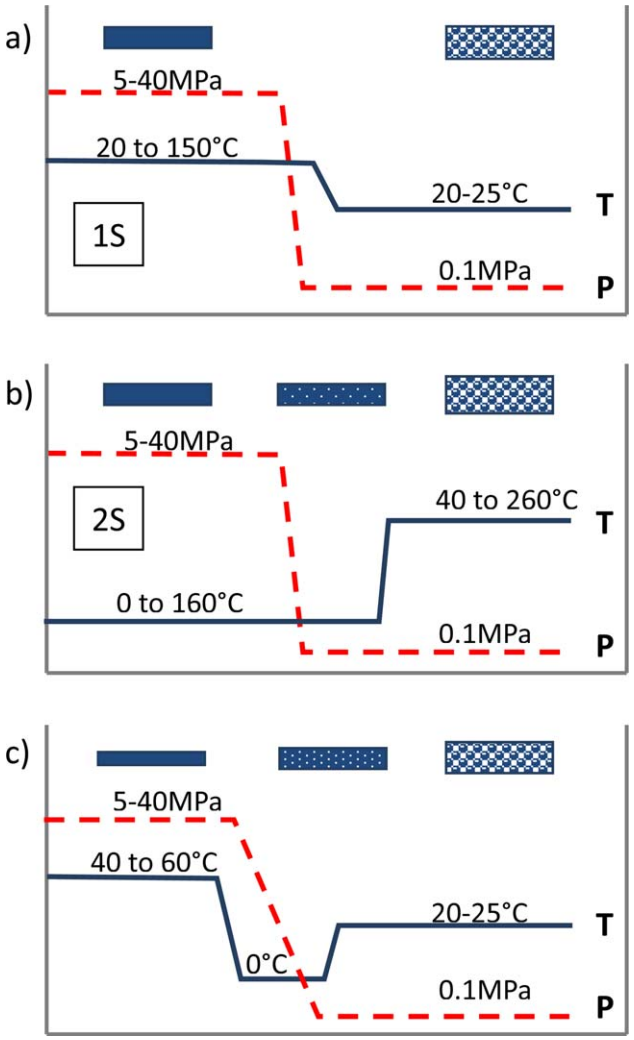

Figure 3. Temperature/pressure profiles commonly used for the production of nanofoam. Top: one-step process; Center: two-step process; Bottom: Modified process with temperature quench before depressurization. [Color figure can be viewed in the online issue, which is available at wileyonlinelibrary.com.]

adapt extrusion foaming to produce nanofoams has been reported in a patent application,[46] illustrated by foams with cell size ca. 300 nm and 70% porosity. No successful production of nanofoam injection molded parts has been reported so far.

POLYMER SYSTEMS FOR NANOFOAMS

For the successful production of nanofoams, the choice of the polymer system will often limit options for the process used, and vice versa. In this section, three general systems are considered:

1. Single phase polymer systems, which can be a single polymer, or a blend of miscible polymers. Both amorphous polymers and semi-crystalline polymers will fall in this category.
2. Nucleated systems and nanocomposites, which include a non-polymeric second phase, usually an inorganic nanoparticle such as clay or silica, into a single phase polymer system
3. Multiphase polymer system, designed to manipulate the partition of CO_2 between several phases to enhance or bypass homogeneous nucleation.

Successful attempts to produce nanocellular foams with CO_2 with the three systems are reported in Table I. The table lists:

- the type of polymer system used. A code indicates the type of sample used: [CF] for solvent cast film (usually a thin film, often a few microns thick, on a substrate such as a silicon wafer); [SF] for self-standing film (thickness < 1 mm); [TS]: thick sheet (thickness>1 mm, usually produced by compression or injection molding)
- the process conditions leading to nanocellular foams, starting with the soaking pressure and temperature range. A code is used to classify the depressurization time: [SD] for slow pressure drop (>1 min); [FD] for fast pressure drop (<1 s) and [ID] for times intermediate between [FD] and [SD]. A second code refers to the type of process: [1S] for one-step foaming; [2S] for two-step foaming (with temperature of thermal conditioning). A temperature quench before depressurization is indicated in the soaking temperature condition (e.g., 40C$\searrow$0C indicates that after CO_2 saturation at 40°C, the temperature was dropped to 0°C before the pressure drop).
- a symbol is used to represent the foam density via the void volume fraction (porosity, p): ● for dense nanofoams ($p < 40\%$); ◉ for intermediate density nanofoams ($40 \leq p \leq 70\%$); ○ for high expansion foams ($p > 70\%$).
- the key characteristics of the nanofoams: their average cell size ϕ_{nm} (or a range if multiple examples of nanofoams were produced), porosity p (calculated from the reported foam density), and cell nucleation density, N_0, in cells per cm^3 of unfoamed polymer. Values of porosity or cell nucleation density not reported in the literature reference were estimated using either eq. (3) for p or eq. (4) below for N_0.

$$N_0 = \frac{6.10^{21}}{\pi \phi_{nm}^3} \frac{p}{1-p} \quad (4)$$

A brief overview of the literature results follows for each type of polymer system. The review is organized per polymer type (amorphous vs. semicrystalline) and per the strategy used (homogeneous system vs. nanocomposite or phase separated system) rather than chronologically.

Single Phase Polymers

PMMA and Retrograde Vitrification. The first polymer considered for the production of foams with very high cell nucleation densities was PMMA.[44] This choice was based on the great affinity of PMMA for CO_2. Under moderate pressure conditions (above 6MPa) sorption of over 15 wt % CO_2 can be achieved, which provides sufficient plasticization to depress T_g below ambient temperature. Condo et al.[47] predicted this could trigger a peculiar behavior they named Retrograde Vitrification, whereby T_g is completely suppressed above a pressure threshold (i.e., PMMA remain in a rubbery regime above this pressure,

Table I. CO_2-Blown Nanocellular Foams Reported in the Literature with Process Conditions and Foam Characteristics (Cell Size, Porosity, and Cell Nucleation Densities in Cells/cm^3)

Polymer type	Process conditions		Nanofoams characteristics	Reference
Single phase polymer systems				
Amorphous polymers				
PS	25 MPa/180C, [FD],[2S at −10C]	◎	<1000 nm/~50% (10^{12})	Janani[99]
PMMA [TS]	27.6-34.5 MPa/40C, [SD], [1S]	●	550 nm/<40% (~10^{12})	Goel[42]
	3.4 MPa/0C, [ID], [2S at 80C]	○	350 nm /~90% (~3.8×10^{13})	Handa[49]
PEMA [TS]	33 MPa/30C, [FD], [2S at 60C]	○	345 nm /79% (1.7×10^{14})	Costeux[64]
P(MMA-co-EMA) [TS]	30 MPa/35C, [FD], [2S at 50-70C]	○	80 nm/80-82% (1.6×10^{16})	Costeux[18,63]
P(MMA-co-tBMA) [TS]	30 MPa/35C, [FD], [2S at 70C]	○	145 nm/78% (2×10^{15})	Costeux[18,63]
Other MMA copolymers [TS] (PFMA, BMA; MSMA)	30 MPa/35C, [FD], [1S]	◎	70-100 nm/50-60% (~5×10^{15})	Costeux[18,63]
PES [SF]	5 MPa/25C, [FD], [2S at 150-200C]	●	40-120 nm /~30% (10^{13}–2×10^{14})	Krause[17,53]
PEI [SF]	4.6 MPa/25C, [FD], [2S at 160-240C]	●	50-80 nm /~30% (10^{13}–3×10^{14})	Krause[53]
PEI [TS]	5 MPa/21C, [ID], [2S at 145-180C]	◎	30-120 nm /30-53% (2×10^{14})	Miller,[57] Chatchaisucha[56]
PEI [TS]	20 MPa/45C, [ID], [2S at 165-205C, 0.1-10 MPa]	◎	40-100 nm /30-60% (>10^{15})	Aher[59]
PI [CF]	5 MPa/25C, [FD], [2S at 260-270C]	●	20-50 nm /<35% (~10^{15})	Krause[54,55]
Miscible blends				
PEMA/SAN [TS]	33 MPa/30C, [FD], [2S at 60C]	◎	95-110 nm /59-68% (3×10^{15})	Costeux[41]
PMMA-co-EA/SAN [TS]	33 MPa/30C, [FD], [2S at 60C]	◎	86-110 nm /60-69% ($2\text{-}5 \times 10^{15}$)	Costeux[41]
PSU/PI [CF]	5 MPa/25C, [FD], [2S at 210-240C]	◎	200-500 nm /~50% (~10^{13})	Krause[55]
Semi-crystalline polymers				
PP [SF]	15 MPa/135-143C, [FD], [1S]	●	150-300 nm / <25% (~10^{12})	Bao[66]
PET	6 MPa/25C,[ID or FD],[2S at 235C]	●	193 nm /<20% (3.4×10^{13})	Li[43]
Nucleated polymer/nanocomposite				
Semi-crystalline polymers				
PLA+clay [TS]	10 MPa/165C, [FD], [2S at 165C]	◎	360 nm /~42% (~1.2×10^{14})	Fujimoto[72]
	28 MPa/110C, [FD], [1S]	●	200 nm /~<20% (2×10^{13})	Ema[28]
HDPE/clay [TS]	8.3 MPa/50C, [ID or FD], [2S at 125C]	●	250 nm /17% (2.9×10^{13})	Lee[74]
PP+MWCNT [TS]	30 MPa/142-144C, [ID or FD], [1S]	●	70-150 nm /10-30% (<2×10^{14})	Ameli[76]
Amorphous polymers				
PC+clay	18 MPa/80C, [FD], [2S at 160C]	●	600 nm /~20% (~10^{13})	Ito[73]
PC+SiO_2	20 MPa/50C, [FD or ID], [2S at 120C]	●	300-500 nm /<20% (6×10^{12})	Zhai[75]
PMMA+SiO_2 [TS]	30 MPa/60C, [FD], [1S]	○	280 nm /77% (3×10^{14})	Costeux[31,62]
PMMA-co-EA+SiO_2 [TS]	33 MPa/40C, [FD], [2S at 80C]	○	180 nm /82% (1.5×10^{15})	Costeux[31,62]
	30 MPa/40C, [FD], [2S at 70C]	○	95 nm /79% (8×10^{15})	
PMMA-co-EMA+POSS [TS]	33 MPa/40-50C, [FD], [2S at 70C]	○	100-120 nm /85% (~10^{16})	Costeux[31,62]

Table I. *Continued*

Polymer type	Process conditions		Nanofoams characteristics	Reference
	33 MPa/35C, [FD], [2S at 55C]	○	65 nm /74% (2×10^{16})	
SAN+clay [TS]	30 MPa/40C↘0C, [ID],[2S at 100C]	◎	300 nm /~40% (~8×10^{13})	Urbanczyk[29]
SAN+POSS [TS]	33 MPa/30C, [FD], [2S at 60C]	◎	200 nm /70% (5.5×10^{14})	Costeux[31,62]
Multiphase polymer systems				
Diblock copolymer:				
PS-*b*-PFMA [CF]	7.5-30 MPa/60C↘0C, [SD], [1S]	●	10-30 nm /~30% (~3×10^{16})	Yokoyama[34,35]
PS-*b*-PFS [CF]	10-30 MPa/60C↘0-40C, [SD], [1S]	●	20-40 nm /<20% (5×10^{15})	Yokoyama[35]
PS-*b*-PMMA [CF]	4.2-8.6 MPa/40C↘0-40C, [SD],[1S]	●	15-40 nm /<20% (9×10^{15})	Taki[79]
PS-*b*-PFDA [SF]	30 MPa/0C, [SD], [1S]	●	~100 nm /30% (7×10^{14})	Reglero Ruiz[80]
PMMA-*b*-PFMA [CF]	8-30 MPa/45C↘0C, [SD], [1S]	●	30-70 nm /<25% (~10^{15})	Dutriez[51]
PMMA + PMMA-*b*-PFMA	34.5 MPa/40C, [FD or ID], [1S]	●	~300 nm /<25% (~10^{12})	Siripurapu[30]
Triblock copolymer:				
PFMA-*b*-PMMA-*b*-PFMA [CF]	8-30 MPa/45C↘0C, [SD], [1S]	●	20-40 nm /<20% (~10^{16})	Dutriez[51]
MAM [TS]	30 MPa/23C, [ID], [1S]	◎	120 nm /55% (~10^{15})	Pinto[85,88]
PMMA+MAM [TS]	30 MPa/23C, [ID], [2S at 80-100C]	●	200-300 nm /<30% (~10^{14})	Reglero Ruiz[45]
	30 MPa/23C, [ID], [1S]	●	~300 nm /~30% (<10^{14})	Reglero Ruiz[82]
	30 MPa/23C, [ID], [1S]	◎	~200 nm /60% (4×10^{14})	Reglero Ruiz[81]
	10-30 MPa/23-50C, [SD or ID], [1S]	◎	100-200 nm /42-58% (4×10^{14})	Pinto[86,87]
	30 MPa/23-40C, [ID], [1S]	◎	130-150 nm /35-45% (~4.10^{14})	Pinto[84]
Immiscible blends				
ABS [SF]	3.4 MPa/0C, [SD], [2S at 60C]	●	470 nm /~25% (~3×10^{12})	Nawaby[102]
PS/PMMA [CF]	8.6 MPa/40C↘20C, [SD], [1S]	●	40-50 nm <20% (~8×10^{14})	Otsuka[38]
PPE/SAN/SBM	5 MPa/40C, [ID], [2S at 180C]	◎	400 nm, ~40% (~10^{13})	Ruckdäschel[36,91]
		●	350 nm, <30% (2×10^{13})	Ruckdäschel[91]
PEEK/PEI	20 MPa/40C, [ID], [2S at 200C]	●	40 nm /~10% (~10^{14})	Ohshima[103]
PC/PLA		◎	40-130 nm	Bao[104]
PP/hSIS [SF]	20 MPa/25C, [ID], [2S at 120C]	●	250 nm /<20% (7×10^{13})	Nemoto[37]
PP/EP rubber [SF]	20 MPa/25C, [ID], [2S at 120C]	●	500 nm < 10%/ (10^{11})	Nemoto[39]
PP/SEBS [SF]	20 MPa/25C, [ID], [2S at 120C]	●	250 nm /<20% (7×10^{13})	Sharudin[89]

Sample type: [CF]: solvent cast film; [SF]: self-standing film (<1 mm); [TS]: thick sheet (>1 mm).
Depressurization: [SD]: slow (>1 min); [FD]: fast (<1 s); [ID]: intermediate between [FD] and [SD].
[1S]: one-step foaming; [2S]: 2-step foaming (with temperature condition).
Foam void volume (porosity): ●: low (<40%) ◎: intermediate (40-70%) ○: high (>70%).

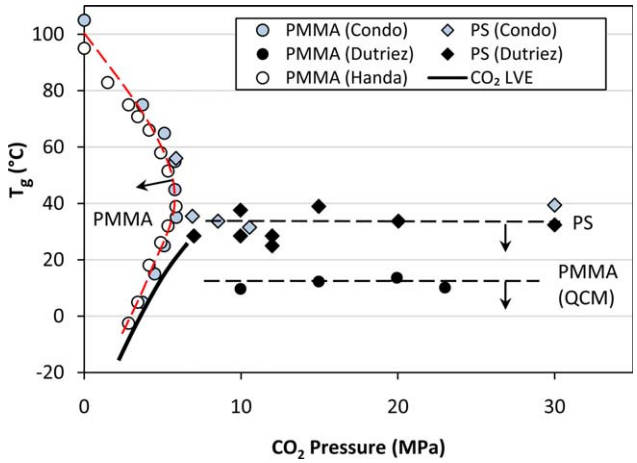

Figure 4. T_g of PS and PMMA. Solid curve represents the liquid–vapor equilibrium for CO_2. Dotted lines are qualitative trends. Arrows indicate the glassy regions. [Color figure can be viewed in the online issue, which is available at wileyonlinelibrary.com.]

irrespective of the temperature), whereas under the threshold pressure PMMA is glassy below a classical upper T_g, but returns to a rubbery state once the temperature is decreased below a lower "retrograde" T_g. This behavior is depicted in Figure 4 (line labeled "PMMA"). Using creep compliance measurements, Condo et al.[48] confirmed their findings experimentally, as did Handa et al.[49] using step-wise DSC experiments. This behavior was only observed for a few polymer/CO_2 systems.[50] It should be noted that the lower T_g branch for these systems is very close to the liquid-vapor transition of CO_2, across which CO_2 density and heat capacity vary sharply, which could interfere with creep and DSC results in this vicinity. Using a quartz crystal resonator, Dutriez et al.[51] observed for PMMA/CO_2 a behavior that resembles that of polystyrene, namely only an upper T_g branch, and a leveling of T_g above a pressure of about 7 MPa [see Figure 4, lines labeled PMMA (QCM) and PS]. According to their results, CO_2 plasticization depresses T_g to about 10°C up to 30 MPa, compared to about 35°C for PS.

The initial approach used by Goel et al.[44] did not rely on retrograde vitrification, since his first successful attempt at producing foams with cells below one micron used a one-step process with CO_2 sorption around 30 MPa and 40°C, i.e. clearly in the rubbery state for PMMA/CO_2.[42] As shown in Table I, this method produced foams with cell nucleation density close to 10^{12}/cm^3 and 550 nm average cell size. Handa et al.[49] exploited the retrograde vitrification of PMMA by choosing pressure and temperature conditions in the narrow region below the lower T_g branch, but above the liquid-vapor phase boundary of CO_2. At −0.2°C, the corresponding pressure is 3.4 MPa, and upon depressurization the PMMA sample came out unfoamed from the autoclave. The authors explained that this is not indicative of the PMMA being glassy under such conditions, but of the low vapor pressure of CO_2 close to the transition line. Upon further exposing the CO_2-laden specimen to a second annealing step at 80°C for 2 min, PMMA foamed and produce low density foams (up to 90% porosity) and cell sizes as low as 350 nm. The improvement in porosity compared to the 1S process of Goel shows the benefit of adding a thermal annealing step. This remarkable achievement (cell density N_0 near 4×10^{13}/cm^3) was seen as a promising sign towards the production of low density nanofoams with cell size approaching 100 nm by homogeneous nucleation. However, the range of conditions and types of polymers for which this strategy can be used are rather limited. Nawaby et al.[50] used the same approach with syndiotactic PMMA and ABS, both found to have the retrograde vitrification behavior, but failed to produce low density nanofoams. The lowest cell size was obtained for ABS (470 nm) but at very low porosity.

High T_g Engineering Plastics. Interest shifted from PMMA to high T_g polymers for the production of separation membranes. In 2001, the pioneering work of Krause[52] showed the benefit of the two-step (2S) process where sorption conditions are chosen at temperature much lower than the T_g of the polymer, in which plasticization is insufficient to render the polymer rubbery. The second thermal conditioning step at temperature close to the T_g of the polymer is thus essential to get nuclei to expand. As shown in Table I, Krause et al. used CO_2 sorption at 25°C under moderate pressures (around 5 MPa) to foam thin films (about 100 μm thick) of PES,[17,53] PEI,[53] and PI[54,55] and produce foams with cells as small as 20 nm. In all cases, however, porosities were very low as the outer surfaces of the membranes were generally left unfoamed. Interestingly, despite the absence of a retrograde behavior for these polymers, the most successful sorption conditions were just above the liquid-vapor line of CO_2, as in Handa's work.[49] The cell nucleation densities were of the order of 10^{14}/cm^3 for PES and PEI, and close to 10^{15}/cm^3 for PI, but the condition and polymer properties did not allow expansion beyond about 30% porosity (1.4 expansion ratio). Despite the low expansion, Krause et al. identified conditions of high CO_2 solubility in PES and PEI under which the core of the membrane could be made bicontinuous[53] (i.e., have a continuous, open pores network). Similar work has been carried out since 2006 by Chatchaisucha et al.[60] and Miller et al.[59,83] with thicker PEI sheets, at pressures and temperature close to values previously used by Krause, but with slower pressure drop rate. Optimization of the 2S foaming conditions led to a slight improvement in foam porosity. A trade-off between cell size and foam expansion was observed, with porosities of about 30% for 30 nm cell size and 53% for foams with 120 nm cells. Very recently, Aher et al.[61] used higher sorption pressures and temperatures (20 MPa/45°C), introduced a clamping force during the high temperature conditioning step, and also adjusted the desorption time (time lapse before the sample is exposed to the high temperature foaming bath). On each side, foams showed a dense skin, an intermediate, low density microcellular layer, and a nanocellular core. The lowest density foams had 52 nm cells in the core, and average porosities on 64% (the porosity of the nanocellular core being likely lower than this number). The idea of constraining the surfaces of the sample during foaming was first applied by Siripurapu et al.[84] on PMMA, although no foam with cell nucleation density higher than 10^{12}/cm^3 was reported at that time.

These attempts at producing high cell nucleation density foams showed the difficulty of producing a sufficient number of nuclei by homogeneous nucleation and of expanding these nuclei to

achieve high porosities ($p > 70\%$). Invariably, when choosing conditions promoting expansion such as slow depressurization,[84] cell size increased, presumably due to coalescence.

High Porosity Nanofoams. Costeux et al. focused on approaches to increase the porosity of nanofoams. Starting in 2009, their initial strategy relied on nucleating additives[85] (discussed in the following nanocomposite section). This initial work helped map out the role of processing conditions but also of polymers structure and properties.[31,68] The key lessons were that high enough CO_2 levels (in excess of 25 wt %) are essential to provide a high level of nucleation while maintaining enough dissolved CO_2 to plasticize the polymer and allow cell growth, and that very fast pressure drop rate was beneficial (their foaming system can be depressurized in a fraction of a second). This strategy is depicted in Figure 2(c).

They designed a series of MMA-based random copolymers containing comonomers with higher CO_2 affinity than MMA, such as ethyl acrylate (EA), ethyl methacrylate (EMA), terbutylmethacrylate (tBMA) etc. covering a range of T_g from 60°C to 120°C.[19] Under the sorption conditions (30 MPa and 35°C), all polymers were in the amorphous state and readily foamed upon depressurization (1S process). Copolymers with T_g between 85°C and 105°C produced nanofoams with cell size between 100 and 200 nm with porosities between 60 and 80%.[18,58] Some higher T_g polymers with high CO_2 solubility, such as MMA-*co*-PFMA, gave foams with 70 nm cell and 60% porosity and remarkably high cell nucleation densities. ($N_0 = 5 \times 10^{15}/cm^3$). When adding a thermal conditioning step below the T_g of the polymer, porosities further increased (78% for the MMA-*co*-tBMA foam conditioned at 70°C). Costeux et al. then applied the same strategy to a high molecular weight MMA-*co*-EMA copolymer to take advantage of the high viscosity to minimize cell coalescence. The optimized 2S process produced a high porosity foam ($p = 82\%$, i.e. over five-fold expansion) with 80 nm cells. The cell nucleation density of $1.6 \times 10^{16}/cm^3$ is the highest reported for homogeneous nucleation.

The MMA-*co*-EMA copolymers ($T_g = 96$°C) were found to be more effective than PEMA ($T_g = 65$°C), which under similar conditions produced foams with 345 nm cells and 79% porosity.[57] The studies concluded that homogeneous nucleation theory was consistent with the experimental trends observed, which was captured in a foaming model.[58]

Miscible Polymer Blends. Miscible blends are often used as a way to produce intermediate properties between those of the blend components. This may be beneficial towards production of nanocellular foams, either to optimize the foaming behavior or to provide a compromise between foamability and foam properties. However, this approach has not been very popular to this day. The first study on miscible blends was reported by Krause et al.,[55] who used PSU/PI blends as a way to investigate the role of CO_2 solubility on microcellular and nanocellular foams properties. They found monotonous dependence of foam properties on the blend composition, and determined nanofoams could be produced for blends of various compositions, as long as the sorption pressure was sufficient to ensure a minimum CO_2 solubility. With a 2S process, at sorption conditions of 5 MPa and 25°C, they obtained nanofoams with cell size between 200 and 500 nm, thus with lower cell nucleation densities that with PI alone.

Costeux et al.[41] used blends of SAN with PEMA or MMA-*co*-EA, in which miscibility could be controlled by the acrylonitrile level in SAN. Using a two-step foaming process with sorption at 33 MPa and 30°C, followed by thermal conditioning at 60°C, they observed that foams with cell size around 90–100 nm and porosities around 60–69% could be produced. Interestingly, in several cases these foams had more homogeneous cell size distribution and smaller cells than foams obtained from either blend component. Addition of as little as 10 wt % MMA-*co*-EA to SAN increased cell nucleation density by several orders of magnitude. Also of interest was the finding that blends with higher CO_2 solubility often gave lower cell densities, a reverse trend compared to predictions of homogeneous nucleation theory. They concluded that homogeneous miscible blends may form separate phases under high CO_2 pressures, responsible for enhanced nucleation densities. Recent studies on phase behavior of similar blends has confirmed the existence of a phase separation, the exact nature of which remains uncertain.[86]

Semicrystalline Polymers. An alternate approach to avoid typical nucleation involves semicrystalline polymers. Polymer morphology in the confined amorphous phase between crystalline lamellae has been shown to be suitable for the generation of nanocells.[62] In particular, a change in the crystalline morphology during foaming, which can be obtained by quenching the polymer from the melt into a metastable state, may generate local stress in the amorphous phase that favors the formation of voids around growing spherulites.[87] Local stresses are also generated in the cell walls during cell growth of microcellular foams, leading to the creation of nanoscale voids in the cell walls.[59,88–90] This behavior has been observed for both HDPE[91] and polypropylene.[90] Such foams do not fit the definition of nanocellular foams, but rather that of open-celled microcellular foams.

Examples of nanofoams made from pure semicrystalline polymers are few. One recent example is due to Bao et al.,[62] who used uniaxially oriented isotactic PP to induce cells in the amorphous space between the crystalline lamellae of shish-kebab structures by a one-step foaming process (15 MPa, ca. 140°C). Sparse cells with size of 150–300 nm were produced, with low porosity ($p < 25\%$). Li et al.[43] used PET, saturated with CO_2 for up to 15 days at 6 MPa and 25°C, followed by a foaming step at 235°C to produce a nanocellular foam with 193 nm cells and 3.4×10^{13} cells/cm^3. Expansion was very limited ($p < 20\%$). Foams produced under different conditions had sandwich structures with microcellular and nanocellular layers.

Nanocomposites

Addition of nanoparticles to foam compositions may offer the dual benefit of assisting nucleation and improving foam mechanical properties. Clays can be easily modified to facilitate intercalation or exfoliation in various polymer matrices, and provide interfaces likely to promote cell nucleation. This motivated a number of foaming studies by the Toyota Technological

Institute (Japan) on PLA/clay nanocomposites[28,63] and later on PC/clay nanocomposites.[66] Fujimoto et al.[63] examined the effect of the dispersion of two different organically modified clays (SBE and ODA) on the foaming behavior of PLA by a two-step high temperature process. Under the optimal foaming temperature (165°C for both sorption and thermal conditioning, which is close to the melting point of PLA) and 10 MPa CO_2 pressure, the nanocomposite in which the modified clay showed the better dispersion (SBE) produced foams with 360 nm and about 42% porosity, compared with 2.6 μm cells for the ODA nanocomposite.

In an attempt to reduce cell size further, Ema et al.[28] foamed the same nanocomposites at higher pressure (28 MPa) and lower temperature (100–110°C) with a one-step process. Interestingly, the behavior of both nanocomposites was similar, producing foams with 200 nm cells. However, the low temperature (about 60°C below the melting point of PLA) prevented foam expansion significantly. Porosities were very low, and the 200 nm cells rather sparse ($N_0 = 2 \times 10^{13}/cm^3$ compared to $1.2 \times 10^{14}/cm^3$ for Fujimoto et al.). They observed by TEM that nanocells were produced at the surface of clay particles, which confirms the heterogeneous nucleation mechanism.

Organically modified clay was also used by Lee et al. to create nanocellular foams in HDPE nanocomposites[64] compatibilized by maleic anhydride-grafted HDPE (15 wt %). They observed that both nanocomposite viscosity and cell nucleation increased with increasing clay levels, while the low CO_2 solubility was largely unaffected and crystallinity decreased. Smallest cells (ca. 250 nm) were obtained for nanocomposites with 3 wt % clay saturated with CO_2 at 8.3 MPa and 50°C and foamed at 125°C. Porosity remained low (17%). Heterogeneous nucleation was identified as the primary mechanism explaining the high cell nucleation density ($3 \times 10^{13}/cm^3$), while the high viscosity suppressed cell expansion.

Urbanczyk et al.[29] compared one-step and modified two-step [see Figure 3(c)] foaming of SAN containing modified clays. An exfoliated clay functionalized with poly(ε caprolactone) was shown to produce a significant increase in cell nucleation in both foaming processes when the temperature was reduced to 40°C, and when the saturation pressure was higher (30 MPa) and depressurization faster. The two-step process led to 300 nm cells with foam porosity around 40% thanks to thermal conditioning close to the T_g of SAN.

Ito et al.[66] also used modified clays in PC nanocomposites compatibilized with SMA. Sub-micron cells (600nm) were produced in a two-step process. Once again, porosities were below 20%. They observed that higher level of clay restricted expansion due to stiffness of the nanocomposite. Zhai et al.[67] examined the effect of nanosized silica particles in PC nanocomposites. SiO_2 domains of about 50 nm promoted heterogeneous cell nucleation, leading to foams with 300–500 nm cells but low porosity. They concluded that higher SiO_2 levels (9 wt %) were beneficial owing to the relative inefficiency of the heterogeneous nucleation process with SiO_2, evidenced by the cell nucleation density in the foams being only 0.01% of the number density of SiO_2 particles in the polymer.

These previous nanocomposite systems make use of polymer matrices not ideally suited for the production of nanofoam. Homogeneous nucleation occurs more readily in polymers with higher affinity for CO_2, which led Costeux et al.[68] to assess the benefit of nanoparticles in the foaming of acrylic polymers. Previously, Siripurapu et al.[30] had produced foams with cells around 1 μm by foaming PMMA/SiO_2 nanocomposites prepared in solution at 34.5 MPa and 120°C. Under conditions where CO_2 solubility in PMMA is higher, Costeux et al.[68] observed that in a one-step foaming process pure PMMA produced very inhomogeneous foams with cells around 900 nm, but that addition of 3 wt % silica nanoparticles led to homogeneous nanofoams with 280 nm cells and 77% porosity.[31] The silica particles with a diameter of 5 nm were added to PMMA by melt blending directly from a silica sol or gel to ensure good dispersion. The same benefit was obtained for MMA copolymers; applying a 2S foaming process to MMA-*co*-EA/SiO_2, with sorption under conditions (30–33 MPa, 40°C) that lead to CO_2 solubilities of 30 wt %, Costeux et al.[31] produced foams with cell size around 100–180 nm and porosities up to 82%. They observed an optimum SiO_2 concentration at 0.5 wt %, and a trend showing smaller cell size (i.e., higher cell nucleation density) for smaller SiO_2 particles size approaching the size of the critical nuclei radius. Similarly to Ito et al.,[66] the effectiveness of particles as nucleation sites was also found to be about 0.1%, presumably due to nuclei coalescence.[32]

Addition of POSS was found to be more effective than SiO_2 with highly CO_2-philic MMA-*co*-EMA copolymer. POSS cages are much smaller in size (0.1 nm) and may not act as true heterogeneous nucleation center. Yet, addition of 0.25 wt % POSS to MMA-*co*-EMA led to low density nanofoams with cell size around 100 nm and record porosities up to 85% (seven-fold expansion). Foams with 65 nm cells and 2×10^{16} cells/cm^3 were also made, albeit with lower porosities (74%). Interestingly, the effect of POSS was found to be more dramatic with SAN, in which the same POSS concentration (0.25 wt %) improved cell nucleation density by 3 orders of magnitude, resulting in 200 nm SAN/POSS foams with 70% porosity.

Ameli et al.[65] turned to multiwall carbon nanotubes (MWCNT) to produce PP nanocomposite foams with microcellular and nanocellular morphologies with improved electrical conductivity. Under optimal conditions (30 MPa, saturation temperature of 142–143°C) in a 1S process, foams with cell size around 70–150 nm were produced, but with low porosity.

In summary, addition of nanoparticles such as clay, SiO_2 or POSS has led to enhancement of nucleation density. The benefit is often more significant at low temperatures. However, to maximize the benefit of nanocomposites, it is preferable to choose conditions where the matrix produces nanofoams by itself. This includes high pressures, low temperatures, fast depressurization, and the choice of a CO_2-philic matrix.

Multiphase Polymer Systems

Organized Templated Systems. As shown in Figure 2(b), two-phase polymer systems provide a mechanism to confine nuclei inside nano domains, especially if a self-assembled structure is used. The concept was first applied with success by Yokohama

et al.[34,35] and Li et al.[92,93] using diblock copolymers of PS with a fluorinated block. PS-*b*-PFMA[34,35,92,93] and PS-*b*-PFS[35] films were cast from solution to generate spherical morphologies with fluorinated domains inside a PS matrix. Foaming was done with the modified 2S process by saturating the diblock films with CO_2 at 60°C and pressures up to 30 MPa to achieve high concentration of CO_2 in the fluorinated domains. The temperature was quenched to 0°C to freeze the PS matrix, the plasticized T_g of which is about 35°C (see Figure 4) before a slow pressure drop. As CO_2 leaves the highly swollen domains, a 10–40 nm void is created in each domain and is maintained stable by the rigidity of the matrix. A very dense foam with 10 nm cells reached a record cell nucleation density of $3 \times 10^{16}/cm^3$. The porosity of other foams is also limited (ca. 30% for PS-*b*-PFMA and less than 20% for PS-*b*-PFS). This is ultimately a limit of the approach based on pure diblocks, where swelling cannot expand the domains enough for their volume to occupy a large fraction during saturation without triggering a phase inversion. Expansion is also hindered by the frozen PS matrix. Other diblock systems, such as PS-*b*-PMMA[69] and PS-*b*-PFDA,[70] were used in a similar process and yielded similar foam structures.

Dutriez et al.[51] also used various PMMA-*b*-PFMA diblocks and PFMA-*b*-PMMA-*b*-PFMA triblocks to produce nanocellular foams with cell size in the range of 20–70 nm and porosities below 25%. Triblock copolymers gave slightly lower cell size and porosity than diblocks. They concluded that the PMMA block needs to be rubbery during saturation and glassy during depressurization to allow for maximum CO_2 swelling and minimum cell collapse. Siripurapu et al.[30] previously compared the effect of graft (PMMA-*g*-PDMS) and block copolymers (PMMA-*b*-PFMA) as additives in PMMA. They observed that both diblocks form micelles in the polymer matrix but also play a role in stabilizing growing bubbles. The finest cellular morphology (ca. 300 nm cells) was obtained for a low molecular weight PMMA-*b*-PFMA added at 2 wt %. The cell nucleation density (and thus the porosity) remained low (ca. $10^{12}/cm^3$).

Reglero-Ruiz et al.[45,73,74] and later Pinto et al.[71,72,75–77,94] conducted a thorough investigation of blends of PMMA with a PMMA-*b*-PBA-*b*-PMMA triblock copolymer (MAM). Addition of 10 wt % MAM was shown to significantly increase CO_2 solubility of PMMA.[71,72] The likely explanation is higher affinity of the PBA block for CO_2, although blends also showed bulk densities lower than both PMMA and MAM[73] which may enhance CO_2 sorption. Reglero-Ruiz et al. foamed blends of PMMA with 10 wt % MAM, which led to dense foams ($P < 30\%$) with 200–300 nm cells* using a 2S process[45] with thermal conditioning at 80–100°C and 300 nm with a 1S process[73] at 30 MPa and 23°C. Foams made with the same 1S process conditions, after removal of their thick densified skin, revealed 200 nm cells, and about 60% porosity in the foam core.[74]

*Note that cell nucleation densities in Ref. 45 are overestimated by more than 2 orders of magnitude.

Pinto et al.[75] adopted the same PMMA/MAM system and systematically studied the effect of pressure from 10 to 30 MPa and MAM content up to 20 wt %, and the relationship between the nanostructure of the blend (density of MAM micelles or vesicles in the PMMA matrix) and the cell nucleation density of the foam. They concluded that micelle density is fairly constant at low MAM levels and is very close to the foam cell density (ca. $4 \times 10^{14}/cm^3$), indicating that nuclei start within MAM micelles. While increasing pressure with PMMA decreased cell size dramatically (as expected from homogeneous nucleation theory), cell size became almost independent of pressure (150–190 nm) once MAM is added at 10 wt %. This important result shows that nanostructured blends with discrete CO_2-philic domains can control nucleation effectively and eliminate homogeneous nucleation in the PMMA matrix and nuclei coalescence. In separate studies, MAM contents from 25 to 75 wt %[77] and 100 wt %[71] were examined. Foams with skinless porosities between 35 and 58% and cell size between 100 and 200 nm were produced with these systems around room temperature. Continuous open pore structures could be obtained by tuning the MAM levels towards 75 wt %.

2-Phase Blends. A number of immiscible blends systems were used as an alternative to self-assembled block copolymers. Nawaby et al. observed that ABS displayed the retrograde vitrification behavior produced high density foams with 470 nm cells under the conditions used by Handa[49] for PMMA. Elastomeric domains (hydrogenated SIS, EP rubber, or SEBS) were also used by Nemoto et al.[37,39] and Sharudin et al.[82] to modify polypropylene. Foams remain dense ($p < 25\%$) with cell size between 250 and 500 nm, but with improved mechanical properties compared to pure PP.

Otsuka et al.[38,95] produced nanoscale PS/PMMA interpenetrating networks (IPN) by *in-situ* polymerization of MMA in PS. PMMA domains were 200 nm in size in blends with 2 : 1 PS:PMMA ratio. Foaming with the process used by Taki[69] for PS-*b*-PMMA, in which the system is cooled below the T_g of the PS phase before pressure release, yielded irregular 50 nm voids that they authors attributed to cells forming in the PMMA phase.

Ruckdäschel et al.[36,79] engineered blends of SAN and PPE compatibilized by SBM triblock copolymers, in which PPE form discrete domains, and the butadiene blocks form interfacial domains between SAN and PPE phases. By a 2S process with sorption at 5 MPa and 60°C and foaming at 160°C, foams with 400 nm cells and 10^{13} cells/cm^3. Slightly smaller cells were obtained with (PPE/PS)/SAN blends compatibilized with SBM.[79]

Summary

Nanocellular foam characteristics from various approaches are summarized graphically in Figure 5, showing a map of expansion ratio (with corresponding porosity) and average cell size. Contour plots for constant cell nucleation density are also represented. The graph illustrates the limitation of pure block copolymer approaches to produce high expansion ratio, even though cell nucleation densities are very high ($10^{15}-10^{16}/cm^3$) and controlled by templating. High T_g polymers provide foams

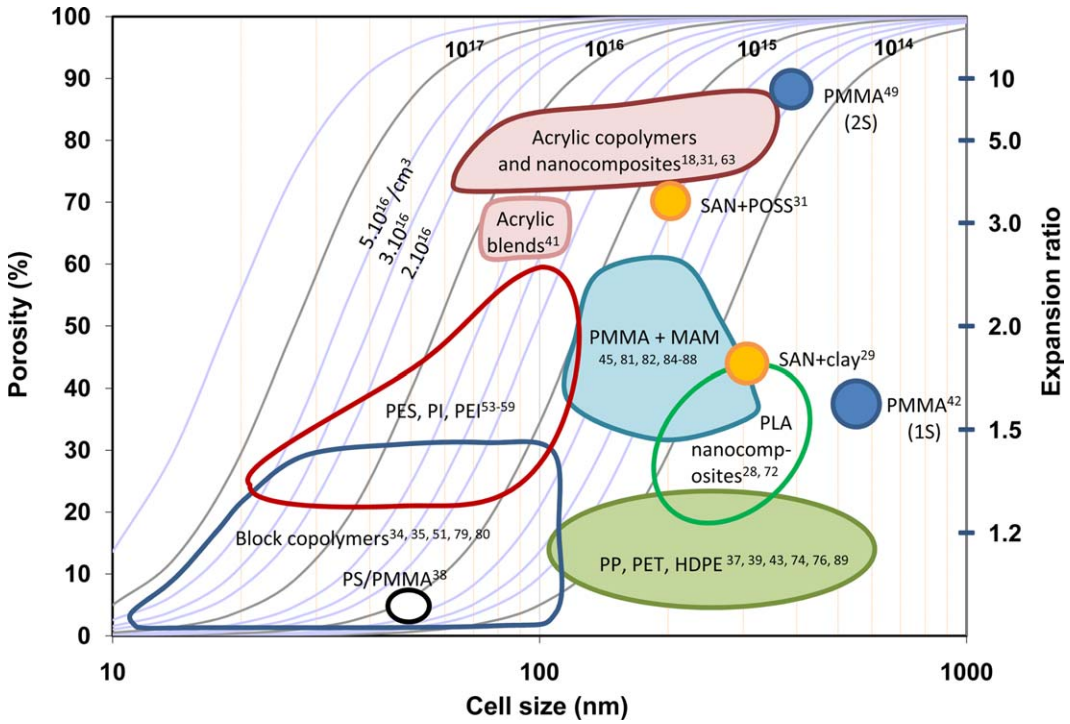

Figure 5. Overview of characteristics (average cell size, porosity, expansion ratio, and cell nucleation density) of nanocellular foams achieved from various polymer systems. [Color figure can be viewed in the online issue, which is available at wileyonlinelibrary.com.]

with similar nucleation density which have recently reached expansion ratios close to 2.5. Acrylic copolymers and their nanocomposites with silica or POSS have resulted in similarly high nucleation densities but with expansion ratios up to 7. PMMA results show the impact of process conditions and the benefit of a thermal conditioning step to maximize expansion. Other approaches such as PMMA+MAM offer the potential to control nucleation density while achieving higher porosity than pure block copolymer (2.5 times expansion).

PROPERTIES OF NANOCELLULAR FOAMS AND POTENTIAL APPLICATIONS

Thermal Conductivity

Hrubesh et al.[3] showed that the TC of organic aerogels is optimal at relative density of about 0.15 (85% porosity). At lower density, heat transfer by conduction through the polymer is reduced, but the materials become more transparent to infrared radiation, which increases TC. Therefore, a common target for nanofoams to provide low thermal conductivity is to minimize cell size below 100 nm (preferably below 75 nm, the mean free path of air molecules) and porosity of 85% or more.[96] Several approaches have led to cells below 100 nm, such as foaming of diblock and triblocks, but with insufficient porosity to meet the 85% target.

Pinto et al.[77] measured gaseous TC on a series of open cells nanofoams from PMMA/MAM blends with medium to high density and demonstrated that it obeys the same cell size dependence as aerogels. This is the first published validation of the Knudsen effect in nanocellular foams, which confirms the expected reduction of heat transfer due to the gaseous phase by a factor 2 to 3 compared to conventional foams. The highest porosity demonstrated for nanofoams with cells of about 100 nm or less is about 85%,[18,31,58,68] which is expected to be suitable to minimize the balance between solid conduction and radiation. No overall TC data have been published to date on such foams but it seems reasonable to assume that low TC foams can indeed be made from low density nanocellular foams. Recent experiments on layered PEI foams structures (microcellular/nanocellular) suggest that nanofoam could have TC as low as 15 mW/m-K,[97] although the measuring technique used does not directly measure the TC of the nanofoam layer.

Mechanical Behavior

Gold nanofoams have been shown to become stronger as the solid is distributed in thinner ligaments, which ultimately produced nanofoams with higher modulus than the nonporous metal.[98,99] The behavior of polymers cannot be transposed from metals, and thus attempts have been made to confirm the mechanical strength benefit of polymer nanofoams. Chen et al.[100] explained that in nanostructured foams, surface effects (residual stress and surface elasticity) have increasingly stronger contribution as the cell size is decreased. The large surface area of nanocellular foam may contribute to the modulus or yield stress sufficiently that it could offset the loss of mechanical properties usually associated with density reduction. In addition, confinement of the solid in the cell walls can result in a reduction of free volume, as evidenced by an increase in the T_g of the polymer in the cell wall,[74] which can also contribute to mechanical strength. Miller et al.[83] compared tensile and impact properties of PEI nanofoams with microcellular foams. They determined that at the same foam density, decreasing cell size

did not affect the tensile modulus and the yield stress, but led to significant increase of toughness and strain at break. PEI nanofoams were also found more ductile, resulting in better impact resistance than both the unfoamed polymer and microcellular foams over the density range studied. Conversely, Sharudin et al.[82] observed for PP and PP/SEBS blends that the yield stress and stress at break were increased compared to unfoamed materials, while the strain at break was unaffected. Thus nanocellular foams have superior properties than microcellular foams at the same porosity, but the nature of the confined polymer, its crystallinity, the density and likely the morphology of the foam determine whether the nanofoams mechanical properties will approach or exceed those of the solid.

Filtration, Separation, and Storage

Open nanoporous membranes made from solvent-based processes have found application as battery separators, in which the transport of ions can be controlled by hindered diffusion in the narrow channels. Films and membranes with connected nanopores have also been used as catalyst support due to their high surface area or as filtration or separation media in which the balance of properties such as particle rejection and flux can be tuned by adjusting the pores size distribution. High surface area nanoporous materials can also be useful for gas capture and storage,[101] catalysis or light harvesting, as reviewed by Dawson et al.[102]

For CO_2-blown nanofoams to be used in such applications, it is necessary to produce bicontinuous foams, as was done by Krause,[53] and to form a foam without integral skin.[56] While such features are easily obtained with solvent-based processes, no successful production of bicontinuous CO_2-blown nanofoams with open surface has been reported.

Other Potential Applications

Low κ dielectric materials have also been produced with polyimide using the porogen approach.[103,104] Krause et al.[54] demonstrated that a CO_2 foaming process could produce nanofoams with dielectric constant below 1.8. Yokoyama et al.[34] showed that optically transparent nanocellular foams can be made, in which the refractive index can be tuned between 1.5 and 1.23 by control of the porosity. Such properties have not yet been exploited.

CONCLUSIONS

Significant progress has been made in recent years in the development of CO_2-blown nanocellular foams. New strategies have been devised to reduce cell size, increase cell homogeneity and lower foam density. Research has been focused on optimizing foaming processes and designing the polymer system to maximize the density of nuclei and control their coalescence. Three main directions have been explored for polymer systems: (i) highly CO_2-philic single phase polymers; (ii) thermoplastic composites with nanofillers; (iii) templated, multiphase polymers.

Pure block copolymer templated systems have successfully produced high cell density foams (10^{14} to 10^{16}/cm^3) by confining nucleation events within dispersed domains, but result in low porosity foams due to minimal cell expansion (10−50 nm). Single polymers with very high T_g also produce very high density foams (porosity < 30%) with small cells and cell densities close to 10^{14}/cm^3. Such materials may become useful for their dielectric or optical properties.

Highly CO_2-philic polymers can easily produce medium density foams (p<50%) with cell nucleation density around 10^{13}/cm^3 and cell size in the 300–500 nm range. However, reducing both cell size and foam density is essential for applications that target insulation. Using nanofillers or by designing the chemistry of the polymers, in particular of those based on methylmethacrylate, it has now become possible to produce 100 nm cell foams with porosities as high as 85% (seven-fold expansion) and cell densities up to 10^{16}/cm^3. Such foams have been shown to exploit the Knudsen effect, and constitute a major step toward production of nanocellular superinsulation.

Hybrid systems, where CO_2-philic domains are distributed within a polymer matrix, produce foams with intermediate properties. They offer the potential benefit of controlling nucleation events (as templated systems) while allowing more foam expansion, at lower pressure or pressure drop rates than necessary for single phase systems. This benefit is yet to be fully realized, as foam expansion remains limited (less than three-fold).

Significant challenges remain for the manufacture of nanocellular foams at a commercial scale, the more substantial of which being the lack of scalability of the widely used solid-state batch foaming process. Continuous nanofoam production is becoming an area of interest for academia, and recent patent literature suggests that the foam industry is also progressing rapidly towards this objective.

ABBREVIATIONS

ABS	acrylonitrile-butadiene-styrene copolymer
BMA	butylmethacrylate
EP	ethylene-propylene rubber
EA	ethylacrylate
PEMA	polyethylmethacrylate
HDPE	high density polyethylene
hSIS	hydrogenated polystyrene-*b*-polyisoprene-*b*-polystyrene
MAM	PMMA-*b*-PBA-*b*-PMMA
MSMA	trimethoxysilylpropyl methacrylate
PBA	polybutylacrylate
PC	polycarbonate
PEEK	Polyether ether ketone
PEI	polyetherimide
PEMA	polyethylmethacrylate
PES	polyethersulfone
PEP	poly(ethylene propylene)
PET	polyethylene terephthalate
PFDA	poly(1,1,2,2-tetrahydroperfluorodecylacrylate)
PFMA	perfluoro-octylethylmethacrylate
PFS	polystyrene-*b*-poly[4-(perfluorooctylpropyloxy)styrene]
PI	polyimide
PLA	poly lactic acid
PMMA	polymethylmethacrylate
POSS	polyhedral oligomeric silsesquioxane

PP	polypropylene
PPE	polyphenylene ether
PS	polystyrene
PSU	polysulfone
SAN	styrene-acrylonitrile copolymer
SBM	styrene-*b*-butadiene-*b*-methylmethacrylate
SEBS	Styrene-*b*-ethylene-butene-*b*-styrene
SMA	styrene-maleic anhydride copolymer

REFERENCES

1. Šupová, M.; Martynková, G. S.; Barabaszová, K. *Sci. Adv. Mater.* **2011**, *3*, 1.
2. Pernites, R. B.; Ponnapati, R. R.; Advincula, R. C. *Adv. Mater.* **2011**, *23*, 3207.
3. Hrubesh, L. W.; Pekala, R. W. *J. Mater. Res.* **1994**, *9*, 731.
4. Zalusky, A. S.; Olayo-Valles, R.; Wolf, J. H.; Hillmyer, M. A. *J. Am. Chem. Soc.* **2002**, *124*, 12761.
5. Hedrick, J. L.; Russell, T. P.; Labadie, J.; Lucas, M.; Swanson, S. *Polymer* **1995**, *36*, 2685.
6. Hedrick, J. L.; Hawker, C. J.; DiPietro, R.; Jerome, R.; Charlier, Y. *Polymer* **1995**, *36*, 4855.
7. du Fresne von Hohenesche, C.; Schmidt, D. F.; Schädler, V. *Chem. Mater.* **2008**, *20*, 6124.
8. Deng, M. L.; Zhou, Q.; Du, A. K.; van Kasteren, J.; Wang, Y. Z. *Mater. Lett.* **2009**, *63*, 1851.
9. Hebb, A. K.; Senoo, K.; Bhat, R.; Cooper, A. I. *Chem. Mater.* **2003**, *15*, 2061.
10. Schwan, M.; Kramer, L. G. A.; Sottmann, T.; Strey, R. *Phys. Chem. Chem. Phys.* **2010**, *12*, 6247.
11. Martini, J. E., The *Production* and Analysis *of Microcellular Foam*, M. Sc. Thesis, Massachusetts Institute of Technology, Cambridge, MA, January **1981**.
12. Youn, J. R.; Suh, N. P. *Polym. Compos.* **1985**, *6*, 175.
13. Hatanaka, M.; Saito, H. *Macromolecules* **2004**, *37*, 7358.
14. Xu, X.; Cristancho, D. E.; Costeux, S.; Wang, Z.-G. *J. Chem. Phys.* **2012**, *137*, 054902.
15. Blander, M.; Katz, J. L. *AlChE J.* **1975**, *21*, 833.
16. Goel, S. K.; Beckman, E. J. *Polym. Eng. Sci.* **1994**, *34*, 1137.
17. Krause, B.; Mettinkhof, R.; van der Vegt, N. F. A.; Wessling, M. *Macromolecules* **2001**, *34*, 874.
18. Costeux, S.; Jeon, H.; Bunker, S.; Khan, I., Nanocellular Foams from Acrylic Polymers: *Experiments; Modeling*, Proceedings of the 10th International Conference on Foam Materials & Technology (SPE FOAMS 2012), Barcelona, Spain, Sept 12–13, **2012**.
19. Kim, Y.; Park, C. B.; Chen, P.; Thompson, R. B. *Soft Matter* **2011**, *7*, 7351.
20. Xu, X.; Cristancho, D. E.; Costeux, S.; Wang, Z.-G. *Soft Matter* **2013**, *9*, 9675.
21. Kim, Y.; Park, C. B.; Chen, P.; Thompson, R. B. *Polymer* **2011**, *52*, 5622.
22. Kim, Y.; Park, C. B.; Chen, P.; Thompson, R. B. *Polymer* **2012**, *54*, 841.
23. Lubetkin, S. D. *Langmuir* **2003**, *19*, 2575.
24. Tomasko, D. L.; Burley, A.; Feng, L.; Yeh, S.-K.; Miyazono, K.; Nirmal-Kumar, S.; Kusaka, I.; Koelling, K. *J. Supercrit. Fluids* **2009**, *47*, 493.
25. Colton, J. S.; Suh, N. P. *Polym. Eng. Sci.* **1987**, *27*, 485.
26. Ramesh, N. S.; Lee, S. T. *Cell. Polym.* **2005**, *24*, 269.
27. Spitael, P.; Macosko, C. W.; McClurg, R. B. *Macromolecules* **2004**, *37*, 6874.
28. Ema, Y.; Ikeya, M.; Okamoto, M. *Polymer* **2006**, *47*, 5350.
29. Urbanczyk, L.; Calberg, C.; Detrembleur, C.; Jérôme, C.; Alexandre, M. *Polymer* **2010**, *51*, 3520.
30. Siripurapu, S.; DeSimone, J. M.; Khan, S. A.; Spontak, R. J. *Macromolecules* **2005**, *38*, 2271.
31. Costeux, S.; Zhu, L. *Polymer* **2013**, *54*, 2785.
32. Zhu, Z.; Park, C. B.; Zong, J. *Annu. Tech. Conf. - Soc. Plast. Eng.* **2006**, *64th*, 2780.
33. Park, C. B.; Baldwin, D. F.; Suh, N. P. *Polym. Eng. Sci.* **1995**, *35*, 432.
34. Yokoyama, H.; Li, L.; Nemoto, T.; Sugiyama, K. *Adv. Mater.* **2004**, *16*, 1542.
35. Yokoyama, H.; Sugiyama, K. *Macromolecules* **2005**, *38*, 10516.
36. Ruckdäschel, H.; Gutmann, P.; Altstädt, V.; Schmalz, H.; Müller, A. H. E. *MRS Proceedings* **2007**, *1056*, HH11-75 doi:10.1557/PROC-1056-HH1511-1575.
37. Nemoto, T.; Takagi, J.; Ohshima, M. *Macromol. Mater. Eng.* **2008**, *293*, 991.
38. Otsuka, T.; Taki, K.; Ohshima, M. *Macromol. Mater. Eng.* **2008**, *293*, 78.
39. Nemoto, T.; Takagi, J.; Ohshima, M. *Macromol. Mater. Eng.* **2008**, *293*, 574.
40. Kumar, V.; Suh, N. P. *Polym. Eng. Sci.* **1990**, *30*, 1323.
41. Costeux, S.; Bunker, S. P.; Jeon, H. K. *J. Mater. Res.* **2013**, *28*, 2351.
42. Goel, S. K.; Beckman, E. J. *Polym. Eng. Sci.* **1994**, *34*, 1148.
43. Li, D.; Liu, T.; Zhao, L.; Yuan, W. *AlChE J.* **2012**, *58*, 2512.
44. Goel, S. K.; Beckman, E. J. *AlChE J.* **1995**, *41*, 357.
45. Reglero Ruiz, J. A.; Tallon, J.-M.; Pedros, M.; Dumon, M. *J. Supercrit. Fluids* **2011**, *57*, 87.
46. Costeux, S. (Dow Global Technologies LLC). Continuous Process for Extruding Nanoporous Foam, PCT *Int. Appl.* WO2013048760, filed September 29, **2011**.
47. Condo, P. D.; Sanchez, I. C.; Panayiotou, C. G.; Johnston, K. P. *Macromolecules* **1992**, *25*, 6119.
48. Condo, P. D.; Johnston, K. P. *Macromolecules* **1992**, *25*, 6730.
49. Handa, Y. P.; Zhang, Z. *J. Polym. Sci., Part B: Polym. Phys.* **2000**, *38*, 716.
50. Nawaby, A. V.; Handa, Y. P.; Liao, X.; Yoshitaka, Y.; Tomohiro, M. *Polym. Int.* **2007**, *56*, 67.
51. Dutriez, C.; Satoh, K.; Kamigaito, M.; Yokoyama, H. *RSC Adv.* **2012**, *2*, 2821.
52. Krause, B. *Polymer Nanofoams*, Ph.D. Thesis, University of Twente, the Netherlands, November **2001**.

53. Krause, B.; Sijbesma, H. J. P.; Münüklü, P.; van der Vegt, N. F. A.; Wessling, M. *Macromolecules* **2001**, *34*, 8792.
54. Krause, B.; Koops, G.-H.; van der Vegt, N. F. A.; Wessling, M.; Wubbenhorst, M.; Van Turnhout, *J. Adv. Mater.* **2002**, *14*, 1041.
55. Krause, B.; Diekmann, K.; van der Vegt, N. F. A.; Wessling, M. *Macromolecules* **2002**, *35*, 1738.
56. Janani, H.; Famili, M. H. N. *Polym. Eng. Sci.* **2010**, *50*, 1558.
57. Costeux, S.; Bunker, S.; Jeon, H., Homogeneous Nanofoams from Synergistic Blends, Proceedings of the 11th International Conference on Foam Materials & Technology (SPE FOAMS 2013), Seattle, WA, Sept 10–11, **2013**.
58. Costeux, S.; Khan, I.; Bunker, S.; Jeon, H. *J. Cell. Plast.* **2014**, doi:10.1177/0021955X14531972.
59. Miller, D.; Chatchaisucha, P.; Kumar, V. *Polymer* **2009**, *50*, 5576.
60. Chatchaisucha, P.; Kumar, V. *Annu. Tech. Conf. - Soc. Plast. Eng.* **2006**, *64th*, 2790.
61. Aher, B.; Olson, N. M.; Kumar, V. *J. Mater. Res.* **2013**, *28*, 2366.
62. Bao, J.-B.; Liu, T.; Zhao, L.; Barth, D.; Hu, G.-H. *Ind. Eng. Chem. Res.* **2011**, *50*, 13387.
63. Fujimoto, Y.; Ray, S. S.; Okamoto, M.; Ogami, A.; Yamada, K.; Ueda, K. *Macromol. Rapid Commun.* **2003**, *24*, 457.
64. Lee, Y. H.; Park, C. B.; Wang, K. H.; Lee, M. H. *J. Cell. Plast.* **2005**, *41*, 487.
65. Ameli, A.; Nofar, M.; Park, C. B.; Potschke, P.; Rizvi, G. *Carbon* **2014**, *71*, 206.
66. Ito, Y.; Yamashita, M.; Okamoto, M. *Macromol. Mater. Eng.* **2006**, *291*, 773.
67. Zhai, W.; Yu, J.; Wu, L.; Ma, W.; He, J. *Polymer* **2006**, *47*, 7580.
68. Costeux, S.; Zhu, L., Thermoplastic nanocellular foams with low relative density using CO_2 as the blowing agent, Proceedings of the 9th International Conference on Foam Materials & Technology (SPE FOAMS 2011), Iselin, NJ, September **2011**.
69. Taki, K.; Otsuka, T.; Waratani, Y.; Ohshima, M., Nano cellular foams of block copolymer thin film, Proceedings of the 5th International Conference on Foam Materials & Technology (SPE FOAMS 2006), Chicago, IL, Sept. 13–14.
70. Reglero Ruiz, J. A.; Cloutet, E.; Dumon, M. *J. Appl. Polym. Sci.* **2012**, *126*, 38.
71. Pinto, J.; Reglero Ruiz, J. A.; Dumon, M.; Rodríguez Pérez, M. A. *J. Supercritical Fluids* **2014**. doi: 10.1016/j.supflu.2014.07.021.
72. Pinto, J. *Fabrication and Characterization of Nanocellular Polymeric Materials from Nanostructured Polymers*, Ph. D. Thesis, University of Valladolid, Spain, May **2014**.
73. Reglero Ruiz, J. A.; Pedros, M.; Tallon, J.-M.; Dumon, M. *J. Supercrit. Fluids* **2011**, *58*, 168.
74. Reglero Ruiz, J. A.; Dumon, M.; Pinto, J.; Rodríguez-Pérez, M. A. *Macromol. Mater. Eng.* **2011**, *296*, 752.
75. Pinto, J.; Dumon, M.; Pedros, M.; Reglero, J.; Rodríguez-Pérez, M. A. *Chem. Eng. J.* **2014**, *243*, 428.
76. Pinto, J.; Dumon, M.; Rodríguez-Pérez, M. A.; Garcia, R.; Dietz, C. *J. Phys. Chem. C* **2014**, *118*, 4656.
77. Pinto, J.; Solórzano, E.; Rodríguez-Pérez, M. A.; de Saja, J. A.; Dumon, M. Thermal Conductivity Transition between Microcellular and Nanocellular Polymeric Foams: Experimental Validation of the Knudsen Effect, Proceedings of the 10th International Conference on Foam Materials & Technology (SPE FOAMS 2012), Barcelona, Spain, Sept 12–13, **2012**.
78. Nawaby, A. V.; Handa, Y. P. *Annu. Tech. Conf. - Soc. Plast. Eng.* **2004**, *62nd*, 2532.
79. Ruckdäschel, H.; Gutmann, P.; Altstädt, V.; Schmalz, H.; Müller, A. H. E. *Adv. Polym. Sci.* **2010**, *227*, 199.
80. Ohshima, M.; Sharudin, R. W.; Nemoto, T.; Takagi, J. *Gummi, Fasern, Kunstst.* **2011**, *64*, 554.
81. Bao, D.; Liao, X.; He, T.; Yang, Q.; Li, G. *J Polym Res* **2013**, *20*, 1.
82. Sharudin, R. W.; Ohshima, M. *Macromol. Mater. Eng.* **2011**, *296*, 1046.
83. Miller, D.; Kumar, V. *Polymer* **2011**, *52*, 2910.
84. Siripurapu, S.; Coughlan, J. A.; Spontak, R. J.; Khan, S. A. *Macromolecules* **2004**, *37*, 9872.
85. Costeux, S. (Dow Global Technologies LLC). Nanoporous Polymeric Foams having High Porosity, PCT *Int. Appl.* WO2011066060, filed November 25, **2009**.
86. Inceoglu, S.; Young, N. P.; Jackson, A. J.; Kline, S. R.; Costeux, S.; Balsara, N. P. *Macromolecules* **2013**, *46*, 6345.
87. Taki, K.; Kitano, D.; Ohshima, M. *Ind. Eng. Chem. Res.* **2011**, *50*, 3247.
88. Sorrentino, L.; Aurilia, M.; Iannace, S. *Adv. Polym. Tech.* **2011**, *30*, 234.
89. Gong, P.; Ohshima, M., Nanoporous Structure on the Cell Wall of Polycarbonate Foams, Proceedings of the 11th International Conference on Foam Materials & Technology (SPE FOAMS 2013), Seattle, WA, Sept 10–11, **2013**.
90. Miyamoto, R.; Yasuhara, S.; Shikuma, H.; Ohshima, M. *Polym. Eng. Sci.* **2013**, doi: 10.1002/pen.23758.
91. Miller, D.; Kumar, V. *Cell. Polym.* **2009**, *28*, 25.
92. Li, L.; Yokoyama, H.; Nemoto, T.; Sugiyama, K. *Adv. Mater.* **2004**, *16*, 1226.
93. Li, L.; Nemoto, T.; Sugiyama, K.; Yokoyama, H. *Macromolecules* **2006**, *39*, 4746.
94. Pinto, J.; Rodríguez-Pérez, M. A.; de Saja, J. A.; Dumon, M.; García, R.; Dietz, C. Relationship between the Nano-Structured Morphology of PMMA/MAM Blends and the Nanocellular Structure of foams Produced from these Materials, Proceedings of the 9th International Conference on Foam Materials & Technology (SPE FOAMS 2011), Iselin, NJ, Sept 14–15, **2011**.
95. Otsuka, T.; Taki, K.; Ohshima, M. *Annu. Tech. Conf. - Soc. Plast. Eng.* **2007**, *65th*, 3002–3005.
96. Schmidt, D.; Raman, V. I.; Egger, C.; du Fresne, C.; Schadler, V. *Mater. Sci. Eng. C* **2007**, *27*, 1487.

97. Sundarram, S. S.; Li, W. *Polym. Eng. Sci.* **2013**, *53*, 1901.

98. Hodge, A. M.; Biener, J.; Hayes, J. R.; Bythrow, P. M.; Volkert, C. A.; Hamza, A. V. *Acta Mater.* **2007**, *55*, 1343.

99. Fan, H. L.; Fang, D. N. *Mater. Des.* **2009**, *30*, 1441.

100. Chen, Q.; Pugno, N. M. *EPL* **2012**, *97*, 26002.

101. Germain, J.; Fréchet, J. M. J.; Svec, F. *Small* **2009**, *5*, 1098.

102. Dawson, R.; Cooper, A. I.; Adams, D. J. *Prog. Polym. Sci.* **2012**, *37*, 530.

103. Charlier, Y.; Hedrick, J. L.; Russell, T. P.; Jonas, A.; Volksen, W. *Polymer* **1995**, *36*, 987.

104. Hedrick, J. L.; Carter, K. R.; Cha, H. J.; Hawker, C. J.; DiPietro, R. A.; Labadie, J. W.; Miller, R. D.; Russell, T. P.; Sanchez, M. I.; Volksen, W.; Yoon, D. Y.; Mecerreyes, D.; Jerome, R.; McGrath, J. E. *React. Funct. Polym.* **1996**, *30*, 43.